Experiments Division

ALBA Project Document No:	EDMS Document No.	Created: 27/10/2006	Pages: 27
EXD-BL22-GD-0006		Modified: 8/6/2007	Rev. No.: 6

Conceptual Design Report

XAS beamline at the
ALBA Synchrotron Light Facility

Prepared by:	*Checked by:*	*Approved by:*
Konstantin Klementiev	**Michael Knapp** **Randolf Butzbach**	**Salvador Ferrer**

Distribution List

Contents

Overview

CELLS is a consortium created to construct and exploit the ALBA synchrotron facility to generate X rays for basic and applied research. The facility, which will be located near Barcelona, will include a 3-GeV low-emittance storage ring able to run in top-up mode, which will feed an intense photon beam to a number of beamlines. These will be placed tangentially to the storage ring and hold the experimental facilities. One of the beamlines, XAS, to be implemented in the first phase of the project, will be devoted to X-ray Absorption Spectroscopy. It will use hard X-rays generated by a multipole wiggler.

This document describes the beamline optics in the logical sequence of defining one element after another. First the optical properties are considered together with geometrical issues, and then the performance under high heat load is addressed. Focusing is analyzed by means of ray-tracing. Finally, some considerations are given for the diagnostics and the future experimental endstation.

To reduce the document size, only short comments are given for each considered issue. To facilitate reading and fast differentiate results from other background information, the following symbols are used throughout the text:

☑   – design choice;

ⓘ   – input information;

☞   – other (rejected) solutions;

☞   – comments on the proposed solution

1   Energy range

☑   2.4–63 keV.

☞   The energy range of the beamline, ideally, should be as wide as possible to propose to the users maximum flexibility in selecting absorption edges. Physically, the usable energy range is limited by source properties, monochromatization approaches (crystal types, number of crystal pairs, geometry of the monochromator etc.), transmittivity of optical elements and by detection approaches (which also depend on the sample).

The lowest energy limit is determined by the largest Bragg angle reachable by commonly used monochromators. Here, the Si (111) crystals are assumed as the most usual ones for moderately hard x-rays. The routinely reachable angle 55.5º corresponds to 2.4 keV (S K-edge). To reach 2.1 keV (P K-edge) is less trivial and needs the Bragg angle 70.3º. The preceding K-edge, of silicon, is not reachable with Si (111) crystals.

The upper energy limit is mostly determined by the magnetic field of the insertion device which, in turn, is limited by technological aspects (magnet type: permanent or superconducting; materials etc.). From the application point of view, this limit can be set based on the following. High-Z elements have too deep K shell to be accessible. Instead, more shallow L_3 edges can be considered. However, the energy range of an L_3 EXAFS spectrum is limited by the presence of the L_2 edge. For elements with Z<70 this length is <1keV, the typical range of EXAFS spectra, thus K-edge is preferable. For Z>70 the K-edges are not generally required, from where the highest energy limit can be set as 63 keV.

2   Optical elements

2.1   Preliminary optics layout before monochromator

☑   multipole wiggler, absorption filters, collimating mirror with cut-off energies 7 and 20 keV.

〰   Combining the requirements:
– high flux;
– large energy range;
– fast energy scanning capability,
the source type for the XAS beamline was selected as *multipole wiggler*. As a wiggler produces high heat load, the power must be effectively removed before the monochromator. Working at low energy, the unwanted high-energy photons can be removed by a *mirror*. Working at high energy, the unwanted low-energy photons can be removed by *absorption filters*.

The mirror before the monochromator has other two functions. It (i) collimates the beam for better energy resolution and (ii) removes high-energy photons which would come through the monochromator as high harmonics and spoil EXAFS. For Si(111) crystals, the first present harmonics are the third order ones. Therefore, starting at 2.4 keV, the first cut-off energy for the mirror must be (<3×2.4 keV) about 7 keV, the next cut-off energy is ~20 keV.

Now, the 3 energy ranges can be specified: 2.4–7 keV (with mirror, without filters), 7–20 keV (with mirror and filters), 20 – ∞ keV (without mirror, with filters). The power outside these ranges is absorbed by the mirror and/or filters and the power inside these ranges is absorbed by the monochromator. As a criterion for determining the period of the wiggler it was considered that the power absorbed by the monochromator had to have an upper limit in order to prevent instabilities in the monochromatic beam.

☞   Two collimation mirrors, one after the other, the 1st (removable from the beam) for high energies, the 2nd for low energies [1].
+: 1 stripe on each mirror (at least on the low-energy one) ⇒ narrow blank (cheaper), better cooling;
–: two benders and two vessels (much space, expensive).

2.2   Multipole wiggler and primary aperture

ⓘ   The wiggler will be placed in a medium straight section, electron beam RMS size = 132h×7.7v µm^2, RMS divergence = 48.5h×5.9v µrad^2.

☑

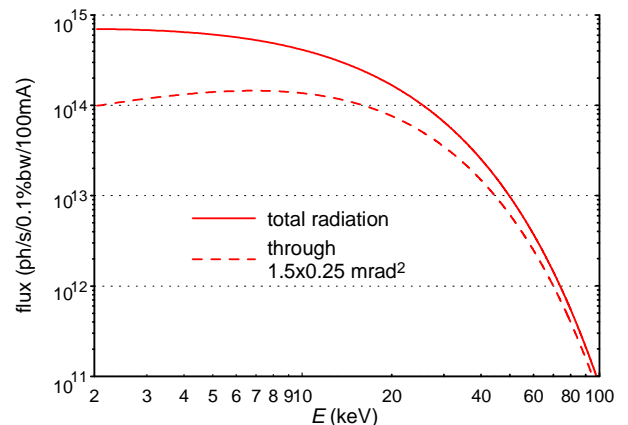| Parameter	Value
total length	1 m
period	80 mm
number of periods	12
minimum gap	12.5 mm
K_{max}	13
maximum field	1.74 T
critical energy	10.4 keV
total power	1.7 kW (@ 100 mA)
	4.3 kW (@ 250 mA)
power in 1.5h×0.25v mrad^2	0.5 kW (@ 100 mA)
	1.3 kW (@ 250 mA)

Fig.1. Flux vs. energy at 100 mA.

The fixed aperture: 1.5h×0.25v mrad^2. The photon source size is nearly independent of the photon energy and approximately equals 320h×18v µm^2, FWHM.
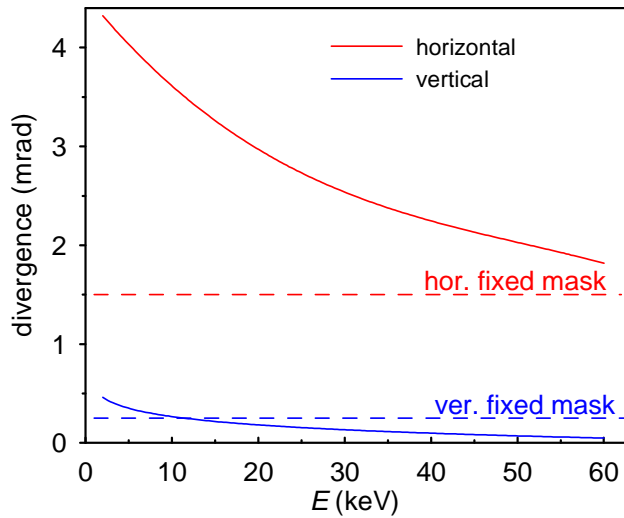

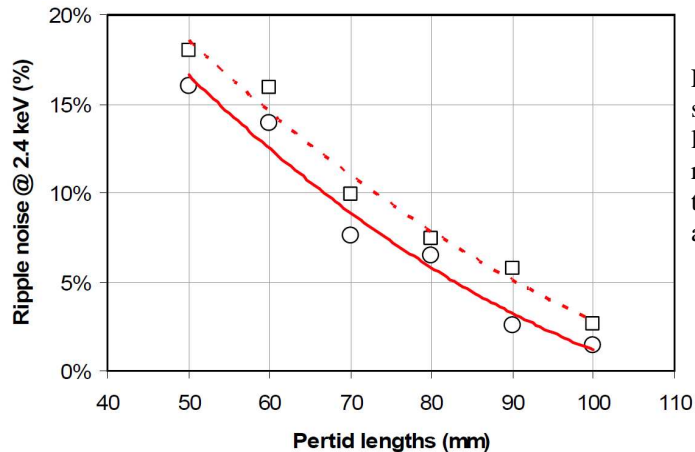Fig.2. Photon beam divergence vs. energy.

Fig.3. Ripple noise in the lower part of the spectrum for a 1-m-long wiggler. Dashed line corresponds to the case of 400 mA (a reduced K value, see below) and solid line to the scenario of 250 and 100 mA in the accelerator.

❧ The wiggler and the beam aperture were optimized [2] under the following constraints: (i) conventional (non-superconducting) technology, (ii) the power absorbed by the monochromator is below 700 W, (iii) the power absorbed by the mirror is below 1 kW, (iv) the ripple noise at lowest energy is below 10 %. The minimum magnetic gap is given as 12.5 mm.

The first constraint appears to be restrictive *at high energies* (20 – ∞ keV). The flux there can be increased by elongating the magnetic period. If it is longer than the optimal one then the magnetic field becomes so high that superconducting technology is needed. This specifies the period.

If the total length is longer than the optimal one then the power load on the monochromator *at low energies* (7–20 keV) overcomes 700 W and the wiggler gap must be open wider. Under these constraints, a wiggler longer than 1m will give a *lower* flux than the optimal one.

Also the incoming beamline aperture was optimized simultaneously. If the whole horizontal fan is collected, the power load at low energies is so high that the period must be decreased, which leads to a decrease of flux at high energies. The optimal horizontal

aperture is the one which does not require shortening of the period. The aperture can, in principle, be decreased further, accompanied with an increase of the total wiggler length. Although this could give a higher flux at high energies, the total power produced by the wiggler would increase linearly with the length. Therefore, this configuration would require opening the gap when working at low energies (7–20 keV) because of too high power on the mirror, which is rather ineffective: a long wiggler but a small aperture and an open gap.

The ripple structure on the low-energy flux curve may cause troubles in monochromator stabilization. Of course, this is not a random structure and a proper stabilization scheme must be able to cope with it. However, the stabilization scheme at a smaller ripple will be easier and more reliable. For a quantitative constraint, consider a detuned monochromator down to 50 – 70 % of the maximum. Then the modulation α in height (ripple) brings to the angle modulation $\alpha\sigma$, where σ is the rocking curve RMS width (@ 2.3 keV, $\sigma\sim100$ µrad). This angle modulation must be compared with the doubled slope error of the mirrors, 2×5µrad (if we take it conservatively). Thus, the ripple must be $r < \sim10\%$.

The storage ring is planned to be operated at a nominal current of 250 mA, and eventually it is foreseen to operate at a maximum of 400 mA. The power values above were calculated for the storage ring current 250mA. For the maximum current, 400 mA, the wiggler gap will have to be opened (i.e the K value is reduced).

The flux was calculated by WS/XOP2.1 code [3] The photon source size and divergence were calculated by Shadow VUI, a part of XOP program [3].

2.3   Collimating mirror

☑   A mirror with 3 stripes: Rh and Pt at the sides and Si at the center with widths of 32 mm, optical length 93 cm, $\Theta = 4.7$ mrad, with bender. For smaller pitch angles used at high energies, the optical length is up to 110 cm. The collimating properties are considered in the ray-tracing section 5.

〰   For the cut-off energies 7 and 20 keV, there exist 2 solutions for the mirror coatings: (i) two stripes, C and Rh(Ru,Mo) at 2.8 mrad; (ii) Si(Al), Pt(Au,Ir), and (to cover the Pt *L*-edges, see the reflectivity curves) Rh(Ru,Mo) at 4.7 mrad. For a mirror at 17.5 m from the source and the vertical beam divergence 0.25 mrad the solution (i) results in a 1.6-meter-long mirror; the solution (ii) results in a 93-centimeter-long mirror.
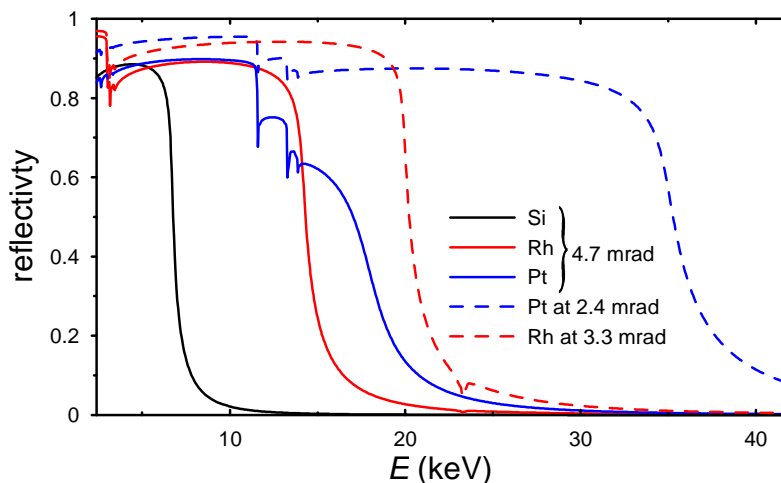

Fig.4. Reflectivity of the three coatings at the incidence angle 4.7 mrad (solid lines) and at 2.4 mrad for Pt and at 3.3 mrad for Rh (dashes).

2.4   Monochromator crystals

ⓘ   The position of the 1st crystal: 19 m from the source, the maximum beam size: 28.5h×5.0v mm².

☑   Double crystal monochromator, liquid N_2 cooling for both crystals, two crystal pairs: Si(111) and Si(311), angle range from 55.5º (2.4 keV) down to 3º, the downstream half of the 1st crystal is 30-mm-long.

〰   Two crystal pairs, Si(111) and Si(311), are foreseen to cover the energies starting from 2.4 keV. Liquid N_2 cooling is required to achieve Darwin width limited energy resolution at high heat load conditions. The second crystals need to be cooled as well otherwise the difference in lattice parameters in the 1st and the 2nd crystals will break the fixed-exit conditions during a long energy scan (a small temperature difference due to high heat load can be neglected in view of nearly zero expansion coefficient of Si around T~125 K).
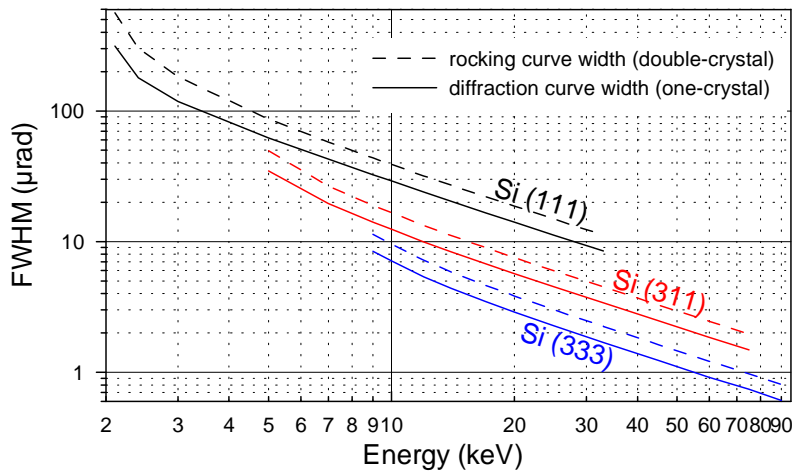

Fig.5. Rocking curve width (dashes) and Darwin width (solid) for different Bragg reflexes on Si crystal. "Diffraction curve" means one-crystal rocking curve, or Darwin curve. "Rocking curve" means two-crystal rocking curve (with only one crystal rocking), obtained by convolution of the diffraction curve with itself. The rocking curves were calculated using XCrystal /XOP[3] at T=77K.

The energy resolution can be found from Fig.5. The Bragg angle range and the crystal sizes can be estimated from the table below. For the angle range: 55.5º–3º, for the longitudinal crystal size: ~60 mm.

E (keV)	Absor. length μ^{-1} (µm)	Si (111)		Si (311)		Si (333)	
		θ_{Bragg} (deg)	longitud. footprint =5.0mm/sin(θ_B)	θ_{Bragg} (deg)	longitud. footprint =5.0mm/sin(θ_B)	θ_{Bragg} (deg)	longitud. footprint =5.0mm/sin(θ_B)
2.1	1.74	70.3	5.3				
2.4	2.44	55.5	6.1				
3	4.38	41.2	7.6				
5	18.0	23.3	12.6	49.2	6.6		
7	47.3	16.4	17.7	32.7	9.3		
9	98.4	12.7	22.7	24.9	11.9	41.2	7.6
10	134.1	11.4	25.3	22.2	13.2	36.4	8.4
12	230.2	9.48	30.4	18.4	15.8	29.6	10.1
14	364.6	8.12	35.9	15.9	18.3	25.1	11.8
17	654.4	6.68	43.0	12.9	22.4	20.4	14.3
20	1074	5.67	50.6	10.9	26.4	17.3	16.8
25	2135	4.54	63.2	8.71	33.0	13.7	21.1
33	5057	3.43	83.6	6.59	43.6	10.4	27.7
45	13423			4.83	59.4	7.57	38.0
60	33574			3.62	79.2	5.67	50.6
65	43416			3.34	85.8	5.24	54.7
75	68846			2.89	99.2	4.54	63.2
90	124192					3.78	75.8

The crystal thickness is determined by the cooling scheme and typically is 2–6 cm.

☞ A channel-cut monochromator. Disadvantages: not as large angle range, more glitches, variable exit height.

Si(220) pair. Cheaper for long crystals but has (440) $\Rightarrow$ more frequent adjustment of the mirrors.

Variable-inclined crystals [4]:

+: one universal crystal pair; decrease of power density; effective slope errors are smaller
−: difficult operation (?).

2.5 Monochromator beam offset

☑ The beam offset must be constant during a scan but may be different at low and high energies. A long 2nd crystal instead of longitudinal translation is preferable. The height of the focusing mirror and the sample must be adjustable.
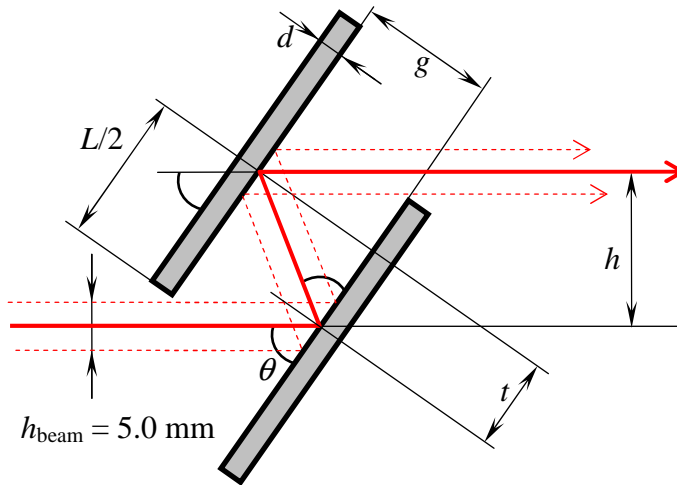

Fig.6. The geometry of a double crystal monochromator.

$h_{\mathrm{beam}} = 5.0$ mm

$$h_{\min} = \frac{L}{2}\sin\theta_{\max} + \frac{h_{\mathrm{beam}}}{2}$$

$$g = \frac{h}{2\cos\theta}$$

$$t = \frac{h}{2\sin\theta}$$

$h_{\min}$ is the minimum beam offset that lets the beam through without shadowing.

$g_{\max}$ is the spacing at angle $\theta_{\max}$; $g_{\min}$ is the spacing at angle $\theta_{\min}$.

$g_{\max} - g_{\min}$ is the perpendicular translation stroke.

$t_{\min}$ is the longitudinal shift at angle $\theta_{\max}$; $t_{\max}$ is the longitudinal shift at angle $\theta_{\min}$.

$t_{\max} - t_{\min}$ is the longitudinal translation stroke.

'L/2' (mm)	$\theta_{\max}=55.5°$								$\theta_{\max}=70.3°$							
	h (mm)	$g_{\max}$ (mm)	$g_{\max}-g_{\min}$ (mm)	$t_{\min}$ (mm)	$t_{\max}-t_{\min}$ (mm) @$\theta_{\min}$=8°	@$\theta_{\min}$=7°	@$\theta_{\min}$=6°	@$\theta_{\min}$=5°	h (mm)	$g_{\max}$ (mm)	$g_{\max}-g_{\min}$ (mm)	$t_{\min}$ (mm)	$t_{\max}-t_{\min}$ (mm) @$\theta_{\min}$=8°	@$\theta_{\min}$=7°	@$\theta_{\min}$=6°	@$\theta_{\min}$=5°
5	6.87	6.07	2.63	4.17	20.5	24.0	28.7	35.2	7.46	11.1	7.33	3.96	22.8	26.6	31.7	38.8
10	11.0	9.70	4.21	6.67	32.8	38.4	45.9	56.4	12.2	18.0	12.0	6.46	37.2	43.4	51.7	63.3
15	15.1	13.3	5.78	9.17	45.1	52.8	63.1	77.5	16.9	25.0	16.6	8.96	51.7	60.3	71.7	87.8
20	19.2	17.0	7.36	11.7	57.4	67.2	80.3	98.7	21.6	32.0	21.2	11.5	66.1	77.1	91.8	112
25	23.4	20.6	8.94	14.2	69.7	81.6	97.5	120	26.3	39.0	25.8	14.0	80.5	93.9	112	137
30	27.5	24.3	10.5	16.7	82.0	96.0	115	141	31.0	46.0	30.5	16.5	94.9	111	132	161
35	31.6	27.9	12.1	19.2	94.3	110	132	162	35.7	53.0	35.1	19.0	109	128	152	186
40	35.7	31.5	13.7	21.7	107	125	149	183	40.4	59.9	39.7	21.5	124	144	172	210
45	39.8	35.2	15.2	42.2	119	139	166	204	45.1	66.9	44.4	24.0	138	161	192	235

From this table the translation stroke of the 2nd crystal can be estimated. If the longitudinal translation t is relatively short, a long 2nd crystal can be used instead. For example, the fixed exit with crystals with 'L/2'=30 mm within the energy range 2.4–65 keV (55.5° for Si(111) down to 5° for Si (333)) will demand a 141-mm-long t translation or at least a 170-mm-long 2nd crystal. Thus, to use a reasonably short 2nd crystal without longitudinal translation, the beam offset should not be constant within the full energy range but rather adjustable when going from the lowest to the highest energies.

2.6   Speed of monochromator

☑   The desired angular speed is 2º/sec. As this is hardly available with existing monochromators, a dedicated quick-scan monochromator is preferred for quick acquisitions. A space for it will be reserved.

☞   Possible ways for fast acquisition:
1) Quick scan = continuous movement of the monochromator;
2) Energy-dispersive XAFS experiments (EDXAFS) = using a polychromator with the sample in focus;
3) Piezo-QEXAFS = tilt of the crystals by piezo-elements.

Drawbacks (corresponding to the acquisition techniques listed above):
1) relatively slow;
2) a) almost impossible to measure intensity before the sample at the same time with the transmitted beam $\Rightarrow$ (very big) problems with the normalization of absorption spectra. This problem was solved by scanning a slit over the beam fan after the polychromator (i.e. sequential data acquisition, known as Turbo-XAFS [10]);
b) the sample must be highly uniform, otherwise rays of different energies 'see' different sample.
3) not fixed-exit $\Rightarrow$ short range (or else the beam height must be corrected, also with piezos, by a downstream mirror or by adjusting the sample height).

Comparison of acquisition time, for 1 keV-long scan at energy 10 keV (i.e. ~ 1° angle range with Si(111)):
1) Quick scan ~10s at X1 beamline at Hasylab;
2) Turbo-XAFS ~0.5s [10];
3) Piezo-QEXAFS: ~0.05s but limited to ~100eV [11] so that the speed is about the same as for 2).
axis angular speed   1°/(0.5 sec) = 2°/sec slew scan
                                             (1°/sec is available by Accel and Cinel)
2nd crystal translation speed   0.1 mm/sec (@ 9 keV)

Notice that the fastest angular motion is needed when the translation motion is slow and *vice versa*.

2.7   Focusing mirror

☑   Two side-by-side toroid mirrors, one with bender, coated by Pt, optical length 1.3 m, $\Theta = 2.4$ mrad; the other without bender, coated by Rh, optical length 1 m, $\Theta = 4.7$ mrad. The focusing properties are considered in the ray-tracing section 5.

☞   In the former versions of the CDR, a single toroid coated by a Rh/Pt bilayer (optical length 1.4 m, $\Theta = 3.7$ mrad.) was planned, as first proposed in Ref. [7]. The reflectivity of such a bilayer is shown in Fig. 7 for different thicknesses of Rh layer (by MLayer/XOP2.1 code [3]).
(i) In a preliminary test of the bilayer mirror at BESSY (μ-Spot BAM beamline) visible steps at the Pt L_3-edge were found on the absorption coefficient measured in transmission mode.
(ii) The pitch angle of such a mirror must be smaller than that of the collimating mirror, which would lead to the length 1.4 m (and some inconvenience with non-horizontal beam propagation at the experiment).
(iii) The focusing for a toroid is only possible at a unique pitch angle; hence the focusing down to sub-millimetre spot size with a bilayer-coated single toroid is only possible for energies up to 20 keV.
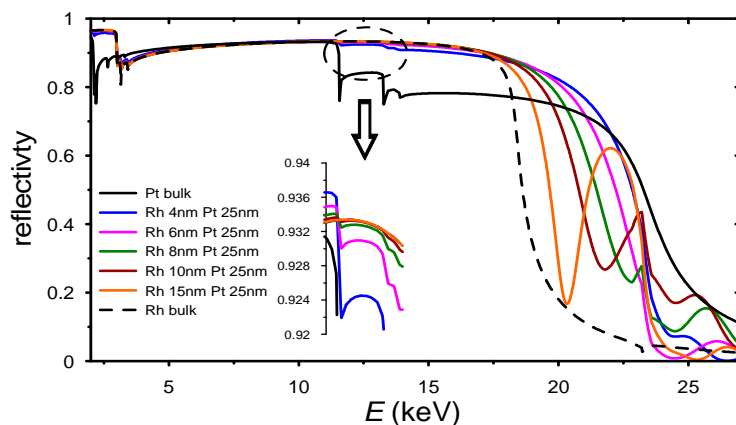Therefore it was decided to use two toroid mirrors.

Fig.7. Reflectivity of a bilayer structure Rh over Pt. With the thickness of Rh > 5nm, the variation of flux at the Pt L_3-edge is <1%.

Sagittally-bent 2nd crystal:
+: independent of mirror's pitch angle (cut-off energy can be adjusted independently);
+: shorter beamline (3:1 relative the 2nd crystal): 25.3m vs. 33.6m needed for mirror focusing.
–: Sensitive to vibrations and clamping; difficult to cool with LN_2.
–: Spoiled energy resolution;
–: A number of bend/pitch/yaw/pitch iterations are required at each energy point $\Rightarrow$ 2.5s dead-time [5];
–: The increase in curvature during bending results in a small change in the separation between the first and second crystals, and hence exit beam height [5] (alternatively, the source-to-crystal distance can be adjusted [6]);
–: "A significant drawback of the current system is that the usual method of detuning the crystals is ineffective for the reduction of harmonic contamination" [6].

2.8   Piezo-elements for monochromator and focusing mirror

A piezo-element on the 2nd crystal. Range: $\pm0.03º \approx \pm0.5$ mrad with < 0.5 µrad resolution. A piezo actuator for the focusing mirror (or a motor-driven fine tuning).

According to [12], whether 1st or 2nd crystal is rocked, the spectrum is splitted into two components which are also shifted from the nominal energy; in the case of piezo on the 2nd crystal one of the two components remains unshifted, therefore rocking the second crystal gives a less distorted energy spectrum.

A rationale to put it onto the 1st crystal: better for an unstable beam but this would complicate excessively the cooling design.

After detuning a crystal by 5–50 µrad, the focus (at 14.6 m away) is shifted by 0.15–1.5 mm. This can be corrected by the focusing mirror pitch angle using a piezo actuator or a motor-driven fine tuning.

2.9   Deflection sequence of mirrors and monochromator crystals

At high energies the mirrors will still be used (see the ray-tracing section 5): at energies 14 – 35 keV with the pitch angle 2.4 mrad, and at energies >30 keV with the pitch angle 1.2 mrad.

«up-up-down-down» deflection sequence for collimation mirror – 1st crystal – 2nd crystal – focusing mirror (or «down-down-up-up», depending on the "standard" deflection way of the monochromator by a given manufacturer). The height of the focusing mirror and of the sample must be adjustable.

Shown below are the cases of different deflection sequences for constant height at the focusing mirror and at the sample. The minimum beam offset at the sample or at the mirror in the sequence «down-up-down-up» is determined by the minimum monochromator offset at the highest energy (i.e. given by the beam size); in the sequence «up-up-down-down» it is determined by the minimum monochromator offset at the lowest energy (i.e. given by the crystal size).
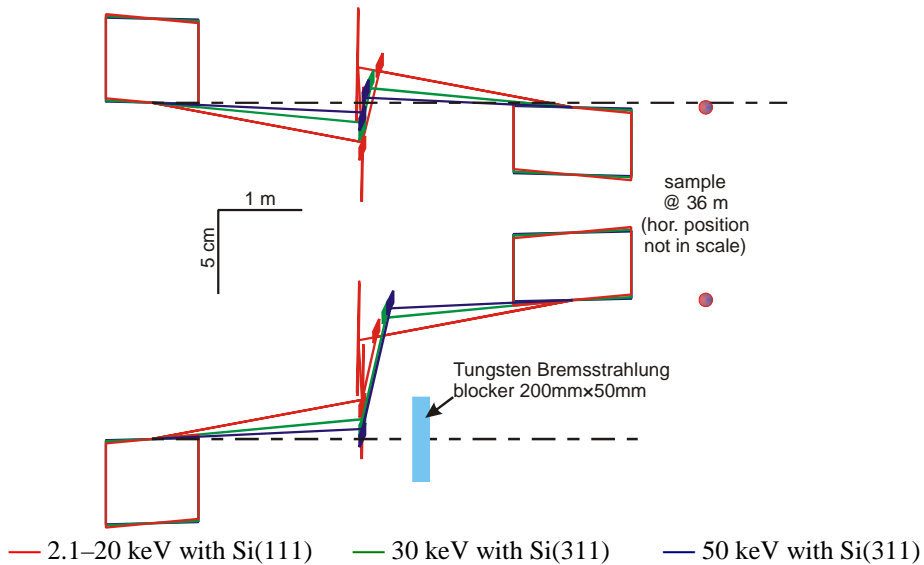

Fig. 8. A comparison of mirror and crystal positions at different energies and deflection sequences.

In the «down-up-down-up» deflection sequence there is no place to put the Bremsstrahlung blocker ⇒ experimental hutch is a white-beam hutch. Thus this sequence is rejected.

The «up-up-down-down» deflection sequence allows the insertion of Bremsstrahlung blocker. However, the translations at high energies are large. Thus the height at the focusing mirror and at the sample must be adjustable.

To be able to insert a 50-mm-thick Bremsstrahlung blocker (the actual dimensions will be given by radiation safety personnel), the monochromator offset must be (i) >15mm when using the collimating mirror at 1.2 mrad (energy setup for E>30 keV); (ii) > 6mm when using the collimating mirror at 2.4 mrad (energy setup for 14<E<35 keV); (iii) at 4.7 mrad there are no restrictions on the smallest monochromator offset besides that coming from the vertical beam size.

3   Power management

ⓘ   The storage ring is planned to be operated at a nominal current of 250 mA, although in the future it is foreseen to operate at a maximum of 400 mA. For the current up to 250 mA the gap of the wiggler will be closed down to the minimum size of 12.5 mm; at a higher current the gap will be opened (the K value will be smaller) to prevent excessive heat load. However, the hypothetical operation with the closed gap at 400 mA is also considered below.

3.1   Power delivered from sources

☑   The power values were obtained by integrating the flux calculated by WS/XOP2.1 and BM/XOP2.1 codes [3].

Source	K				P total (W)				P through aperture[**] (W)			
	100 mA	250 mA	400 mA	400 mA, MG[*]	100 mA	250 mA	400 mA	400 mA, MG[*]	100 mA	250 mA	400 mA	400 mA, MG[*]
MPW	12.976	12.976	9.328	12.976	1718	4295	3551	6872	515	1287	1452	2060
BM									17	42		68

[*] MG = minimum gap 12.5 mm
[**] 1.5h×0.25v mrad^2

3.2   Power distribution on optical elements

ⓘ   Materials considered so far as candidates for absorption filters:

	CVD diamond www.cvd-diamond.com	Sigradur K	Sigradur G	Al
		www.htw-germany.com		
Density (g/cm^3)	3.52	1.54	1.42	2.7
Thermal conductivity (W/mK)	2000	4.6	6.3	237
T max	1500°C [*]	1000°C	3000°C	melting 660°C
Available dimensions	thickness 10 - 2000 μm, diameter up to 100 mm	thicknesses 0.5 – 6 mm, films: 60μm, 100μm, 140μm and 180μm	thicknesses 0.5 – 6 mm	any

[*] graphitization: 700°C in an oxygen containing and 1500°C in an inert atmosphere

The power values were calculated by XPower/XOP2.1 code using the flux calculated by WS/XOP2.1 and BM/XOP2.1 code [3].
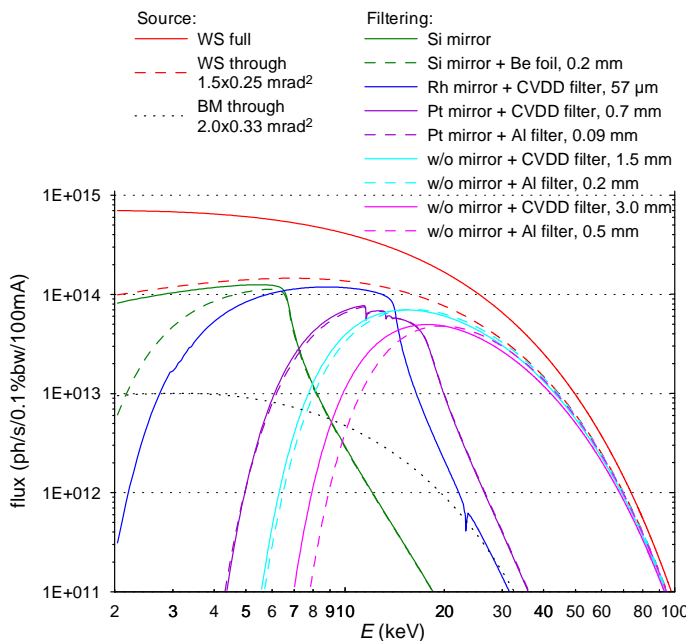

Fig.9. Flux before the monochromator for different combinations mirror+filter.

☑

Energy range (keV)	Absorption filter	Power absorbed in filter (W)				Mirror **)	Power absorbed by mirror (W)				Power transmitted to mono (W)			
		@100 mA	@250 mA	@400 mA	@400 mA, MG*)		@100 mA	@250 mA	@400 mA	@400 mA, MG*)	@100 mA	@250 mA	@400 mA	@400 mA, MG*)
<6	–	–	–	–		Si	402	1004	966	1608	113	283	486	452
	Be, 0.2 mm	55	138	244	220		391	977	926	1564	69	172	282	276
6–14	CVD-diamond, 57 µm	78	196	341	312	Rh	247	618	469	988	189	473	643	756
	Sigradur K, 140 µm	81	202	350	324		247	617	467	988	187	468	634	748
14–18	CVD-diamond, 0.7 mm	213	532	802	852	Pt	191	478	328	764	111	277	323	444
	Sigradur G, 1.75 mm	213	533	803	852		192	478	327	768	110	276	321	440
	Al, 0.09 mm	210	526	805	840		196	490	334	784	108	271	313	432
>~18	CVD-diamond, 1.5 mm	275	687	976***)	1100***)	–	–	–	–	–	240	600	476	960
	Sigradur G, 3.7 mm	274	686	975***)	1096***)		–	–	–	–	241	601	477	964
	Al, 0.2 mm	269	672	976***)	1076***)		–	–	–	–	246	615	476	984
>~22	CVD-diamond, 3.0 mm	338	846	1133***)	1353***)	–	–	–	–	–	177	442	319	707
	Sigradur G, 7.5 mm	339	848	1135***)	1356***)		–	–	–	–	176	440	317	703
	Al, 0.5 mm	339	848	1156***)	1357***)		–	–	–	–	176	439	295	702

*) MG = minimum gap 12.5 mm.
**) Mirror @ 4.7 mrad: Si, Rh and Pt stripes.
***) plus ~50W from BM.

4 attenuators are planned for different energy ranges. In going to higher energies, the attenuators will not be replaced but added one after another starting with the thinnest one. This will share the absorbed power approximately equally among the inserted filters. Each filter will then absorb ~300W. The materials for the filters have not been decided yet.

4   Thermoelastic calculations by Finite Element Analysis

ⓘ   The Finite Element Analysis (FEA) was performed by L. Nikitina and M.Quispe (CELLS, Engineering Division) using ANSYS code.

The FEA of the collimating mirror and of the 1st monochromator crystal has been done. The absorption filters are to be considered in some weeks.

The influence of the thermal deformations on the optical properties is considered in the ray-tracing section 5.

4.1   Collimating mirror

ⓘ   Power absorbed by the mirror was calculated by repetitive runs of WS/XOP2.1 code [3] for a small aperture translated over the beam footprint 1020×28.5 mm^2.
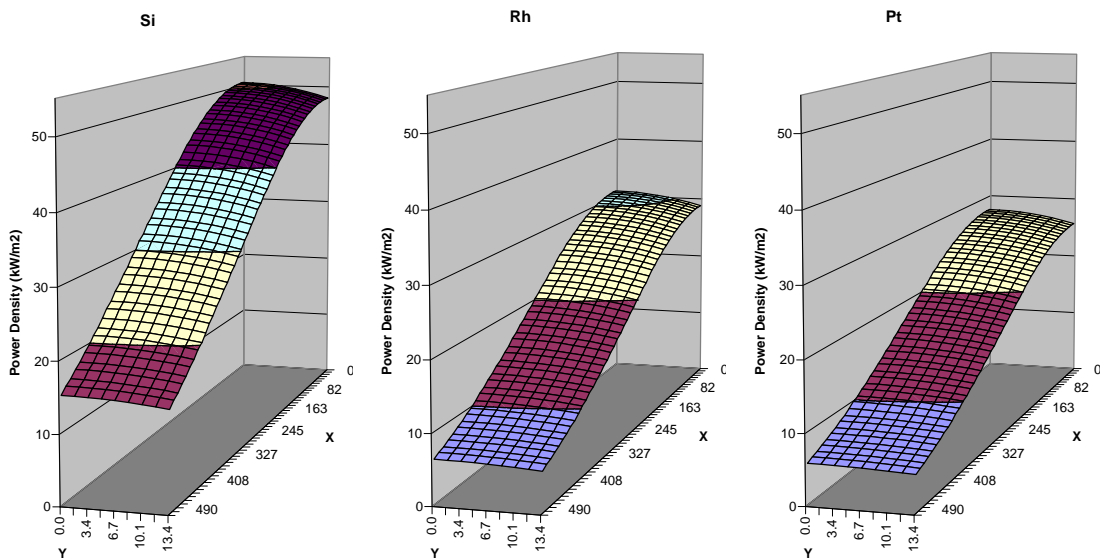
Fig.10. The power densities for one quarter of the footprint.

Total power absorbed at the different stripes: Si: 1005 W, Rh: 555 W, Pt: 494 W

☑   The calculated deformations are smaller for the side-cooled silicon mirror than for the GlidCop directly-cooled mirror. The Si stripe should be positioned in the center. For side cooling, the copper cooling blocks must have the water tubes as close as possible to the mirror surface. Laminar water flow is sufficient.

The FEA results are provided as separate files in directory http://www.cells.es/Divisions/Experiments/XAS/

file	mirror type	case
END_BL22OPFEA_ER_0001_v03.pdf	GlidCop, direct cooling	Si-stripe
END_BL22OPFEA_ER_0002_v03.pdf	GlidCop, direct cooling	Pt-stripe
END_BL22OPFEA_ER_0003_v03.pdf	Si, side cooling	Si-stripe
END_BL22OPFEA_ER_0004_v01.pdf	GlidCop, direct cooling	conceptual study of boundary conditions
END_BL22OPFEA_ER_0005_v01.pdf	Si, side cooling	Rh-stripe
END_BL22OPFEA_ER_0006_v01.pdf	Si, side cooling	Pt-stripe
END_BL22OPFEA_ER_0007_v01.pdf	Si, side cooling	preliminary studies of external cooling for mirror (laminar and turbulent flow, different stripe positioning, fine and coarse heat application, number of cooling tubes)

Example: Si mirror with side cooling, Si stripe in the middle (DMC at 7 keV).
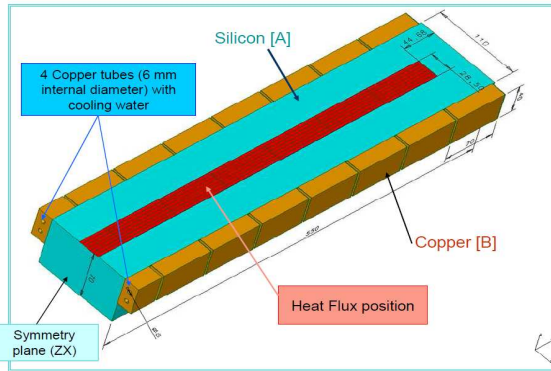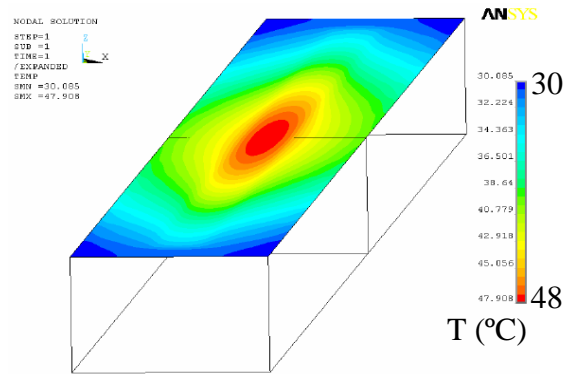

Fig.11. The geometry of the mirror.

Fig.12. The surface temperature distribution.

T_{max}<48ºC, dz_{max} = 8.2 µm. The deformation (shown in Fig. 13) consists of a global bending, that can be approximated by a circular cylinder shape of radius R = 19 km, and a small bump on top of it. The global bending can be corrected by a bender. RMS slope error after correction for global circular bending = 3.4 µrad:
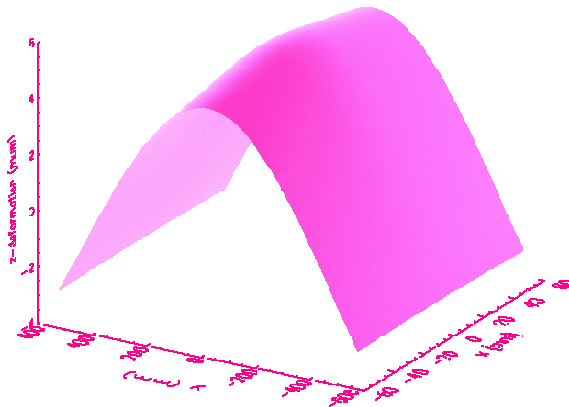
Fig.13. The calculated perpendicular deformation.
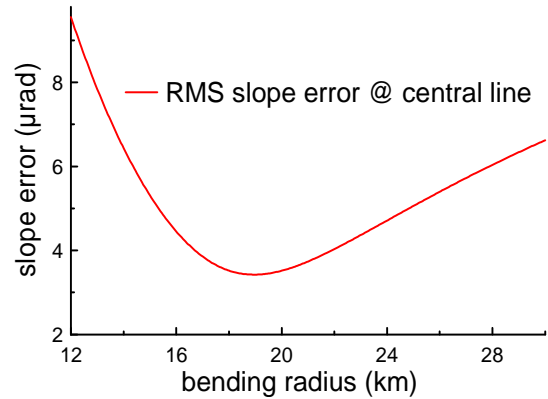
Fig.14. The thermal slope error vs bending radius.

4.2   1st crystal

Si(111) crystal. Dimensions: 60×60×110 mm³. Thermal conductance 6000 W/m² K for the liquid nitrogen – copper interface, 6000 W/m² K in sliding contact between copper and silicon, temperature dependent material properties taken from Ref. [8]. Liquid nitrogen temperature was taken to be 77 K (at atmospheric pressure) or 92 K (at ~4 bar).

Three cases of power load were considered:

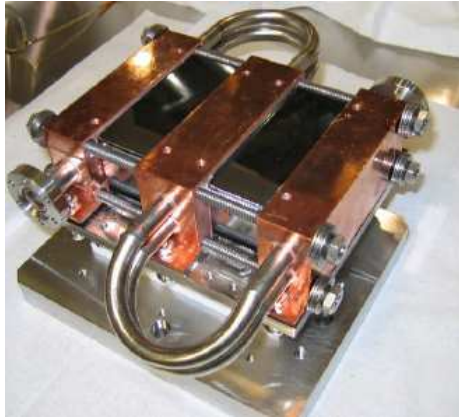|	description	E, θ_B	footprint (mm²)	P abs (W)
case A	preliminary studies for surface and volume absorption, differently tabulated thermoconductivity coefficients, etc. T_{min} = 77K.	2.1 keV, 70.3º	33.8h×5.0v	282 at 250 mA
case B	*the highest power density*	2.1 keV, 70.3º	33.8h×5.0v	452 at 400 mA
case C	*the highest total power*	~6 keV, 20º	33.8h×13.9v	748 at 400 mA and minimum gap

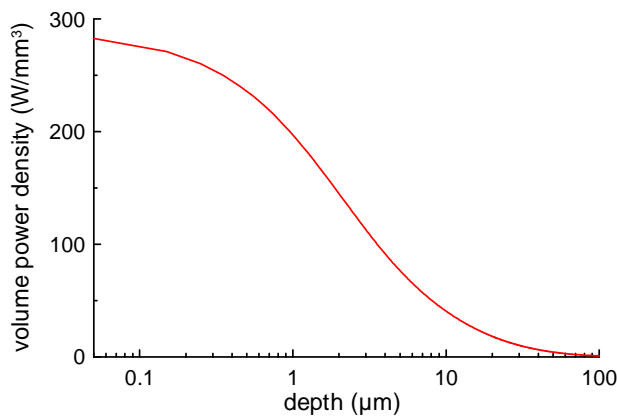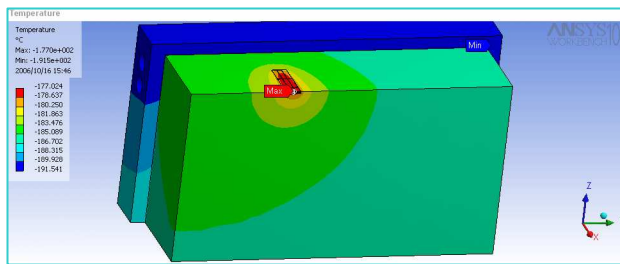Fig.15. An example of the cooling scheme taken from Accel.

Fig.16. Case A. Volume power density absorbed in the 1st crystal at different thickness.

Fig.17. Case A. Temperature distribution for surface heat absorption. Maximum surface power density ~5 W/mm^2

Fig.18. Case A. Temperature distribution for volume heat absorption. Maximum volume power density ~250 W/mm^3 in the 1st 1-µm-thick layer.
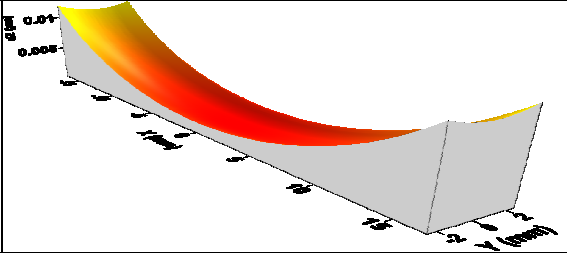
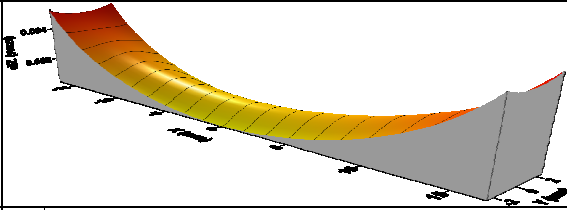

T_{max}=−177.0 ℃ (96.2K)
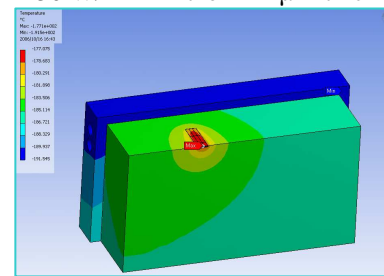
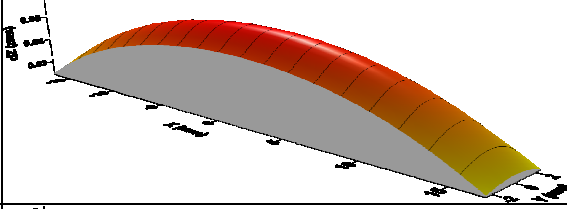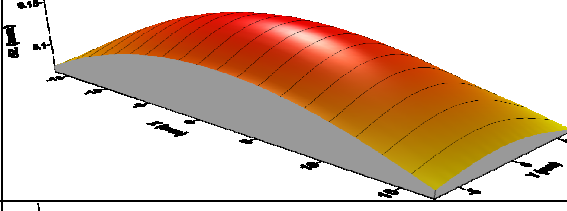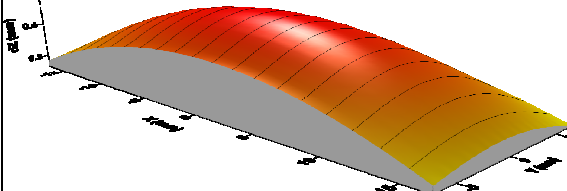

T_{max}=−177.1℃ (96.1K)

The surface and the volume heat application give very close results when considering the first layer to be 10-µm or-µm-thick. Superficial absorption is assumed for further calculations.

Fig.19. Case A. Temperature distribution for surface heat absorption and one-half of the crystal thickness:
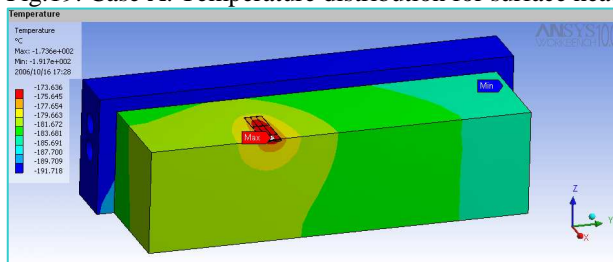
T_{max}=−173.6 ℃ (99.6K)

Results of thermoelastic calculations (see section 5.10 for ray-tracing)

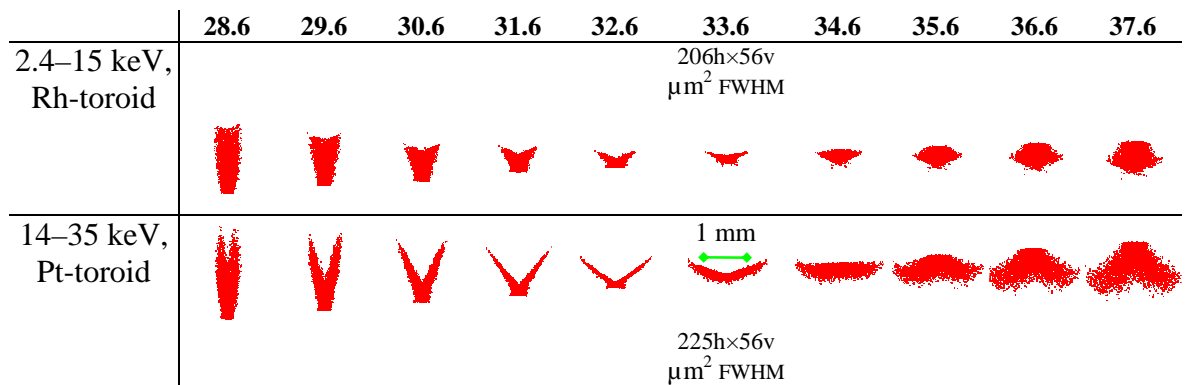|	T_{max} (K)	deformed surface	deformation difference along longitudinal middle line (x=0)	deformation difference along sagittal middle line (y=0)
case A, $T_{min} =$ 77K	96.2		-0.002 µm	-0.011 µm
case B, $T_{min} =$ 77K	111		0.0011 µm	-0.0035 µm
case B, $T_{min} =$ 92K	132.5		0.01 µm	0.023 µm
case C, $T_{min} =$ 77K	132		0.05 µm	0.08 µm
case C, $T_{min} =$ 92K	156		0.13 µm	0.18 µm

5 Ray-tracing

ⓘ The ray-tracing was done using Shadow VUI/XOP2.1 code [3] which is a graphical user interface to Shadow2.3.0 [9]. For getting the beam images, 25000 rays were used. To calculate the FWHM sizes, 100 successive runs were accumulated. For all the beam images below, except the footprint pictures, the vertical and horizontal scales are always equal.

5.1 Focus position

ⓘ As found by MacDowell et al. [7], the optical system collimating mirror + toroid focusing mirror has a "magic" configuration at 2:1 horizontal demagnification which eliminates astigmatic coma.

☑ Horizontal demagnification for the focusing mirror 2:1= 22.4m (focusing mirror to source) 11.2m (sample to focusing mirror).

〰 Beam image for two different toroids: Rh-coated at $\Theta_{CM}=\Theta_{FM}$=4.7 mrad and Pt-coated at $\Theta_{CM}=\Theta_{FM}$=2.4 mrad. Meridional radius R and sagittal radius ρ here are variable and depend on the focus position (first row, in meters). $R = 2q/\sin\Theta$, $\rho = 2pq\sin\Theta/(p+q)$.

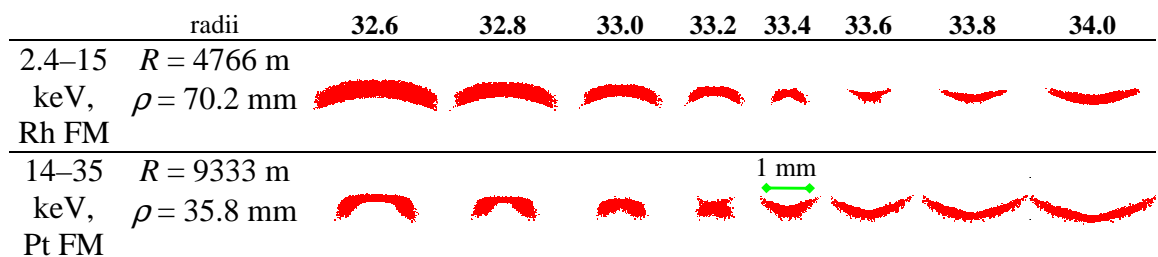|	**28.6**	**29.6**	**30.6**	**31.6**	**32.6**	**33.6**	**34.6**	**35.6**	**36.6**	**37.6**
2.4–15 keV, Rh-toroid						206h×56v µm² FWHM				

Demagnifications at 33.6 m: 22.4:11.2=2 in horizontal and 17.5:11.2=1.56 in vertical. The diffraction-limited imaging would give 160h×11.5v µm².

5.2 Focus size at different sample positions

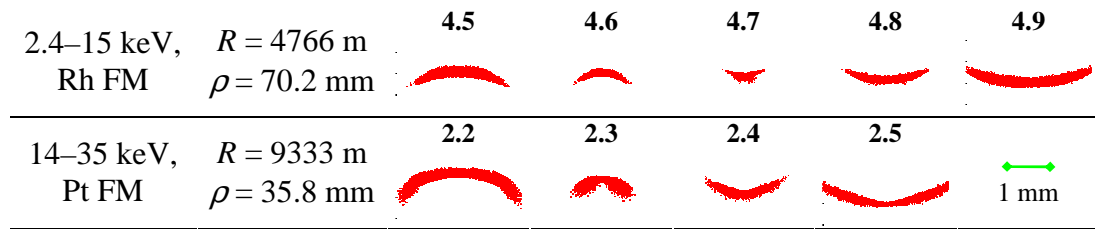☑ The sample must be positioned within +10–20 cm from the optimal position.

〰 Scan of the sample position (in meters, first row) for the focus at 33.6 m.

	radii	**32.6**	**32.8**	**33.0**	**33.2**	**33.4**	**33.6**	**33.8**	**34.0**
2.4–15 keV, Rh FM	$R = 4766$ m $\rho = 70.2$ mm								
14–35 keV, Pt FM	$R = 9333$ m $\rho = 35.8$ mm								

5.3 Focus size for different angles of focusing mirror

Scan of the FM pitch angle (in mrad, bold font) for the focus at 33.6 m

		4.5	**4.6**	**4.7**	**4.8**	**4.9**
2.4–15 keV, Rh FM	$R = 4766$ m $\rho = 70.2$ mm					

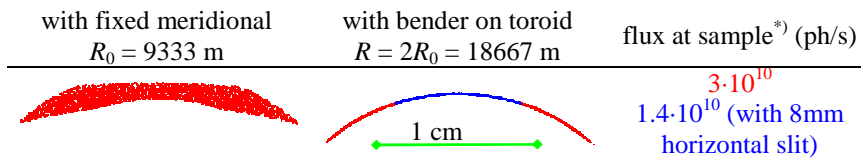|		**2.2**	**2.3**	**2.4**	**2.5**	
14–35 keV, Pt FM	$R = 9333$ m $\rho = 35.8$ mm					1 mm

5.4 Focusing at high energies

☑ Also at high energies the mirrors should be used to improve energy resolution and reduce the beam size. The Pt-toroid mirror needs a bender.
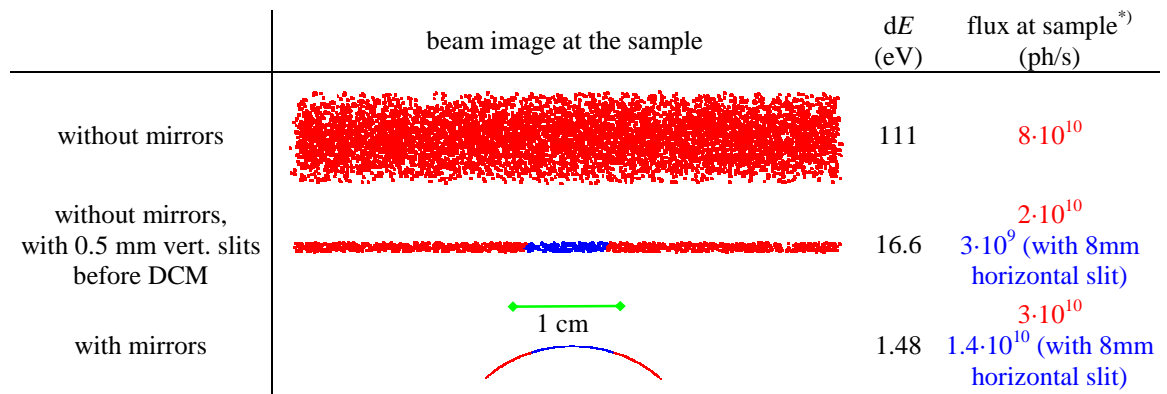
fixed sagittal radius $\rho_0 = 35.8$ mm, $E=50$keV:

with fixed meridional $R_0 = 9333$ m	with bender on toroid $R = 2R_0 = 18667$ m	flux at sample[*] (ph/s)
	1 cm	$3 \cdot 10^{10}$ $1.4 \cdot 10^{10}$ (with 8mm horizontal slit)

[*] the source flux was calculated by WS/XOP, the transmittivity by Shadow VUI/XOP.

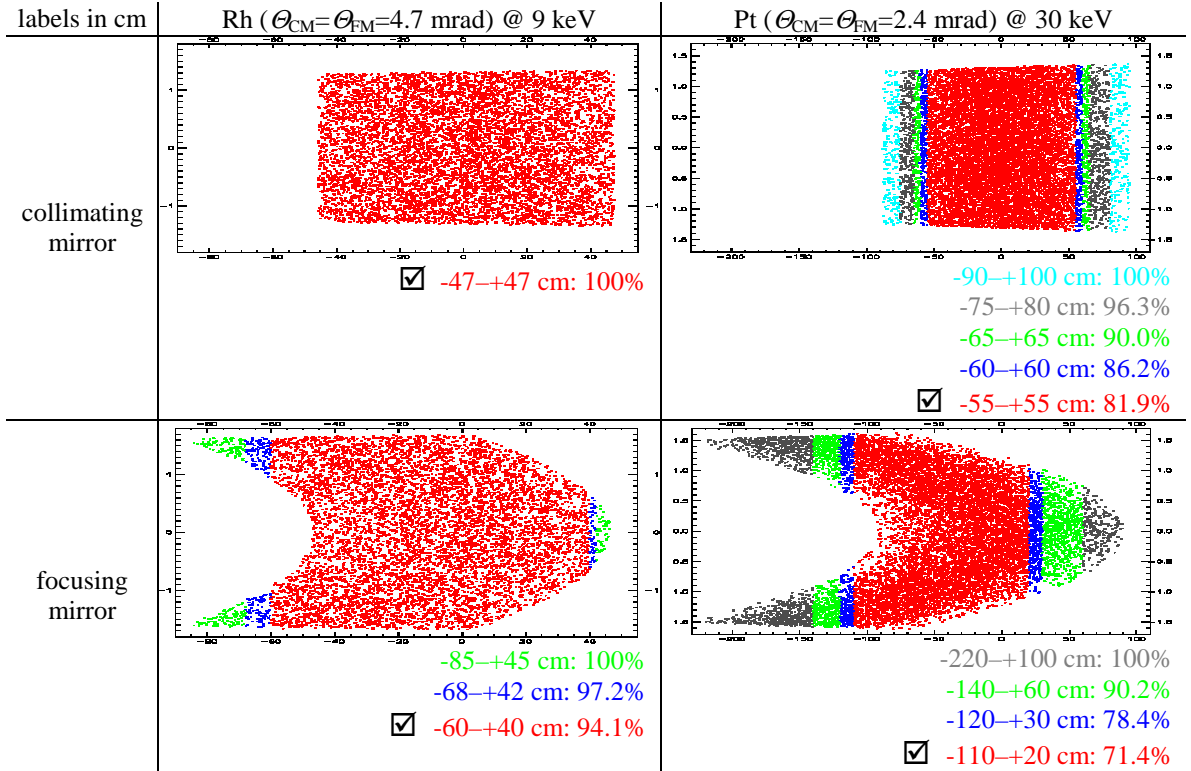Without mirrors, energy resolution is much worse (example @ $E=50$keV):

	beam image at the sample	dE (eV)	flux at sample[*] (ph/s)
without mirrors		111	$8 \cdot 10^{10}$
without mirrors, with 0.5 mm vert. slits before DCM		16.6	$2 \cdot 10^{10}$ $3 \cdot 10^{9}$ (with 8mm horizontal slit)
with mirrors	1 cm	1.48	$3 \cdot 10^{10}$ $1.4 \cdot 10^{10}$ (with 8mm horizontal slit)

[*] the source flux was calculated by WS/XOP, the transmittivity by Shadow VUI/XOP.

The reduction of the beam divergence with slits is, in principle, also sufficient for acceptable energy resolution, as the width of K-edges at $E\sim50$ keV is ~23 eV.

5.5 Footprints on mirrors

☑ The dimensions marked as ☑ in the table below were selected for the mirrors and used in ray-tracing.

〰 Intensity percentage collected by the four mirrors of different sizes.

labels in cm	Rh ($\Theta_{CM}=\Theta_{FM}$=4.7 mrad) @ 9 keV	Pt ($\Theta_{CM}=\Theta_{FM}$=2.4 mrad) @ 30 keV
collimating mirror	 ☑ -47–+47 cm: 100%	 -90–+100 cm: 100% -75–+80 cm: 96.3% -65–+65 cm: 90.0% -60–+60 cm: 86.2% ☑ -55–+55 cm: 81.9%
focusing mirror	 -85–+45 cm: 100% -68–+42 cm: 97.2% ☑ -60–+40 cm: 94.1%	 -220–+100 cm: 100% -140–+60 cm: 90.2% -120–+30 cm: 78.4% ☑ -110–+20 cm: 71.4%

5.6 Influence of roughness on collimating properties

☑ The influence of roughness is negligible if the RMS roughness is below 10 Å.

〰 Two different PSD functions (Power Spectral Density) were modelled:
a) Gaussian Power Spectrum with $\sigma_x = \sigma_y = 100$ cm^{-1};
b) from a profile with normal statistics and Gaussian correlation function with correlation length 50 µm.
10 Å rms roughness was assumed in both cases.

The resulted increase in focus size was <3 µm in horizontal and ~1 µm in vertical directions; the intensity loss was <2%.

5.7 Influence of fabrication slope errors on collimating properties and energy resolution

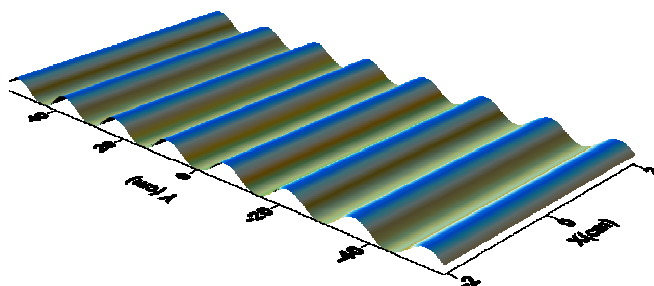☑ 2.5–5 µrad rms slope error is acceptable for the collimating mirror.

ⓘ

Fig.21. The model surface used in ray-tracing to simulate the fabrication figure error. The period of the wave is 150 mm [13], the rms slope error was scaled as 0, 2.5, 5, 10, 25 and 50 µrad.

〰

rms slope error (µrad)	Si stripe, 6 keV, Si(111) Θ=4.7 mrad 1 mm	Rh stripe, 13 keV Si(111) Θ=4.7 mrad 1 mm	Pt stripe, 30 keV Si(311) Θ=2.4 mrad 1 mm	Pt stripe, 50 keV Si(311) Θ=1.2 mrad 8 mm
0				
FWHM size (μm^2)	207×56	208×53	225×56	187
dE (eV)	0.77	1.76	0.90	1.43
flux at sample (ph/s)	$9 \cdot 10^{12}$	$1 \cdot 10^{13}$	$5 \cdot 10^{11}$	$1.4 \cdot 10^{10}$
2.5				
FWHM size (μm^2)	209×182	209×181	225×185	425
dE (eV)	0.76	1.77	3.71	9.25
flux at sample (ph/s)	$9 \cdot 10^{12}$	$1 \cdot 10^{13}$	$5 \cdot 10^{11}$	$1.5 \cdot 10^{10}$
5				
FWHM size (μm^2)	210×337	211×334	225×339	475
dE (eV)	0.77	2.96	6.92	9.97
flux at sample (ph/s)	$9 \cdot 10^{12}$	$1 \cdot 10^{13}$	$5 \cdot 10^{11}$	$1.3 \cdot 10^{10}$
10				
FWHM size (μm^2)	220×639	221×637	241×638	749
dE (eV)	1.21	5.5	13.41	9.99
flux at sample (ph/s)	$9 \cdot 10^{12}$	$1 \cdot 10^{13}$	$5 \cdot 10^{11}$	$1.3 \cdot 10^{10}$
25				
FWHM size (μm^2)	287×1549	289×1549	421×1552	2000
dE (eV)	2.7	12.4	32.77	9.99
flux at sample (ph/s)	$9 \cdot 10^{12}$	$1 \cdot 10^{13}$	$4 \cdot 10^{11}$	$1.4 \cdot 10^{10}$

The width of a K edge at energy E can be roughly estimated as $2 \cdot 10^{-4} \cdot E$. Thus, the energy resolution must be <1.2 eV at 6 keV, <2.6 eV at 13 keV, <6 eV at 30 keV, <10 eV at 50 keV. These requirements are all fulfilled with rms slope error 2.5 µrad and partially fulfilled with rms slope error 5 µrad. The latter must be taken as the upper tolerable slope error.

5.8 Influence of fabrication slope errors on focusing properties

☑ As the slope errors on the focusing mirror do not spoil energy resolution, 5–10 µrad rms meridional slope error is acceptable for the focusing mirror. The sagittal slope error may be as high as 1000 µrad, which is far above usual production values.

rms **meridiaonal** slope error (µrad)	Rh-toroid 6 keV Θ=4.7 mrad 1 mm	Pt-toroid 30 keV Θ=2.4 mrad 1 mm	Pt-toroid 50 keV Θ=1.2 mrad 8 mm
0			
FWHM size (µm^2)	207×56	225×56	63
flux at sample (ph/s)	9·10^{12}	5·10^{11}	1.4·10^{10}
2.5			
FWHM size (µm^2)	208×183	225×187	244
flux at sample (ph/s)	9·10^{12}	5·10^{11}	1.4·10^{10}
5			
FWHM size (µm^2)	208×338	227×342	387
flux at sample (ph/s)	9·10^{12}	5·10^{11}	1.4·10^{10}
10			
FWHM size (µm^2)	210×646	225×652	704
flux at sample (ph/s)	9·10^{12}	5·10^{11}	1.4·10^{10}
25			
FWHM size (µm^2)	223×1557	255×1573	1000
flux at sample (ph/s)	9·10^{12}	5·10^{11}	1.4·10^{10}

rms **sagittal** slope error (µrad)	Rh-toroid 6 keV Θ=4.7 mrad 1 mm	Pt-toroid 30 keV Θ=2.4 mrad 1 mm	Pt-toroid 50 keV Θ=1.2 mrad 8 mm
0			
FWHM size (µm^2)	207×56	225×56	63
500			
FWHM size (µm^2)	249×59	238×58	174
1000			
FWHM size (µm^2)	329×64	272×61	168
2500			
FWHM size (µm^2)	647×87	428×80	175
5000			
FWHM size (µm^2)	990×138	681×127	207

5.9   Influence of thermal distortions of collimating mirror on focusing properties

☑ The thermal distortions can be corrected by re-bending the mirror. The resulting radius is rather small; pre-shaped cylinder is probably required.

⤳ Example of thermal deformations from section 4.1 (Si stripe, 1 kW absorbed power, monochromator @ 7keV).

w/o bump	with bump						
R = 7447 m	7447 m	7000 m	6500 m	6000 m	5350 m	5000 m	4500 m
1 mm							
dE = 0.91 eV	2.10 eV	1.86 eV	1.54 eV	1.13 eV	0.93 eV	0.96 eV	1.09 eV
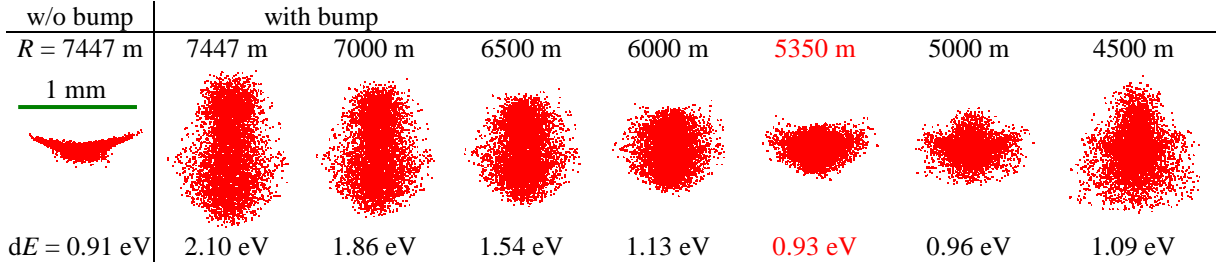
The CM with nominal radius R_{CM} must be re-bent as $1/R'_{CM} = 1/R_{CM} + 1/R_{bump}$ (this is so because the z deformations and all $d^n z/dy^n$ are additive, and $d^2 z/dy^2 = 1/R$). Here the thermal bump has the global radius R_{bump} as determined from FEA (section 4.1).

Focus size and energy resolution for the 3 stripes (all other imperfections are ignored):

	Si			Rh			Pt		
	w/o bump	with bump	re-bent	w/o bump	with bump	re-bent	w/o bump	with bump	re-bent
R_{bump} (m)	∞	19000		∞	39600		∞	45100	
R_{CM} (m)	7447	7447	5350	7447	7447	6268	7447	7447	6392
focus FWHM (μm^2)	206×56	240×943	210×135	208×53	212×487	208×115	225×52	238×407	226×95
$dE^{*)}$ (eV)	0.91	2.10	0.93	1.76	3.78	1.79	0.52	2.74	0.72
at E (keV)	7 with Si (111)			13 with Si (111)			18 with Si (311)		

After re-bending:
a) the horizontal size recovers;
b) *the vertical size nearly doubles* in comparison to the unloaded case;
c) the energy resolution recovers with Si(111) but not with Si(311). However, the energy bandwidth 0.72 eV obtained for the Pt-stripe at 18 keV is still much less than the edge widths near this energy: ~3.5 eV for K-edges and ~10 for L_3-edges.

As the Pt-case is most demanding for smaller thermal bump, the Pt stripe is put closer to one of the cooling sides of the collimating mirror (on the other side is Rh-stripe, Si being in the middle).

5.10   Influence of thermal distortions of 1st crystal on focusing

☑ The focus distortions are acceptable even in the case of the highest power density and the highest total power. In the latter case the liquid nitrogen temperature (and thus the pressure of it) should be kept as low as possible. If this is technically difficult, the power load must be decreased by opening the wiggler gap, as it was planned at the stage of the wiggler optimization for the highest current 400 mA.

To some extent, the crystal bump can be corrected by the CM.

Examples of thermal deformations from section [4.2](#).   <u>1 mm</u>

	w/o bump	$T_{min} = 77K$	$T_{min} = 92K$
case B *the highest power density* (2.1 keV, 282W) focus FWHM (µm²) dE (eV)	 206×56 0.195	 202×64 0.195	 200×284 0.197
case C *the highest total power* (6 keV, 748W) focus FWHM (µm²) dE (eV)	 206×56 0.77	 208×407 0.79	 234×960 1.17

The crystal bump can be to some extent corrected by re-bending the CM. The correct estimation of re-bending requires a self-consistent calculation of "bending radius + footprint on crystal + power load on crystal + ANSYS". The examples below are just rough estimations as they are not self-consistent, i.e. the re-bending was only considered in ray-tracing, without re-calculating the power load and thermal deformations.
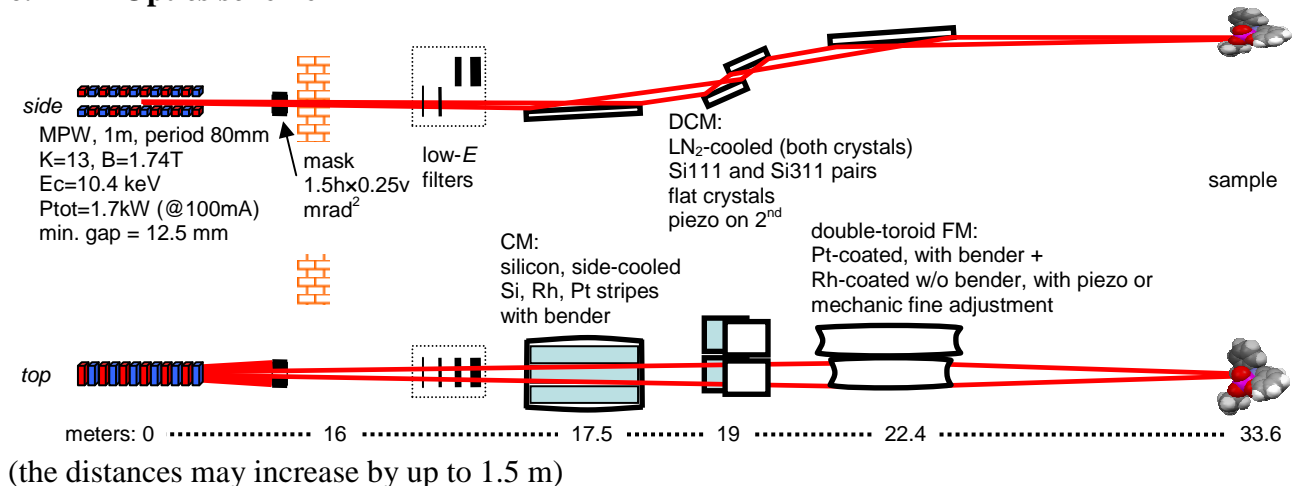
	w/o bump	$T_{min} = 77K$	$T_{min} = 92K$
case C corrected by CM focus FWHM (µm²) dE (eV)	 $R_{CM} = 7447$ m 206×56 0.77	 $R_{CM} = 6400$ m 204×92 0.75	 $R_{CM} = 5200$ m 201×100 0.77

5.11   Dependence on wiggler position

The length of the straight section is 3.2 m. The magnetic length of the wiggler is 1m. It can be shifted off center of the straight section by 0.8 m downstream (to the center of the downstream half of the straight section) in order to make the beamline shorter by one half of this movement.

☑ This movement results in increase of the electron beam rms size from 132h×7.4v µm² to 136h×8.9v µm² and of the focus FWHM size by~ 10h×4v µm². If this shift does not influence the electron beam dynamics, it should be taken.

6   Summary of optics layout

6.1   Optics scheme

side

MPW, 1m, period 80mm
K=13, B=1.74T
Ec=10.4 keV
Ptot=1.7kW (@100mA)
min. gap = 12.5 mm

mask
1.5h×0.25v
mrad²

low-E
filters

CM:
silicon, side-cooled
Si, Rh, Pt stripes
with bender

DCM:
LN₂-cooled (both crystals)
Si111 and Si311 pairs
flat crystals
piezo on 2nd

double-toroid FM:
Pt-coated, with bender +
Rh-coated w/o bender, with piezo or
mechanic fine adjustment

sample

top

meters: 0 ·········· 16 ·········· 17.5 ········ 19 ········· 22.4 ············ 33.6

(the distances may increase by up to 1.5 m)

6.2 Modes of operation and performance

Energy range (keV)	Filter[*]	CM stripe	mirror angle (mrad)	DCM crystals	FM toroid	beam fwhm h×v[**]	flux (ph/s)
2.4 – 7	–	Si	4.7	Si(111)	Rh	206×56 µm^2	1·10^{13} @7 keV
6 – 15	57 µm	Rh	4.7	Si(111)	Rh	208×53 µm^2	1·10^{13} @9 keV
7 – 20	0.7 mm	Rh	3.3	Si(311)	Rh	8×0.4 mm^2	1·10^{12} @18 keV
14 – 20	0.7 mm	Pt	2.4	Si(311)	Pt	225×56 µm^2	1·10^{12} @18 keV
18 – 35	1.5 mm						5·10^{11} @30 keV
30 – 70	3.0 mm	Pt	1.2	Si(311) Si(333)	Pt	8×0.4 mm^2	1.4·10^{10} @50 keV

[*] CVD-diamond
[**] without fabrication and thermal induced figure errors

7 Preliminary considerations for diagnostics

Parameters to monitor:

– position before the collimating mirror. Initially it was planned to do this with thermocouples on the primary slits. Now, these slits have been shifted to the front-end. So that another monitoring capability is needed (4 blade XBPM?)

– position before DCM by guard slits with thermocouples.

– intensity after DMC before FM. Not obligatory but a very useful option to feed the monochromator stabilizator, Mostab, instead of the first ionization chamber. This has two advantages: (i) decoupling of intensity and vertical position (the change in the vertical beam position due to the piezo-adjustment will be up to 0.5 mm near the focus); (ii) the stabilization will not be influenced by the Pt *L*-edges of the focusing mirror coating. It is desirable to have two devices for this: (a) a 4-diod setup with fluorescence foils for low energies and (b) a CVD-diamond plate (as a solid-state ionization chamber) for high energies.

– fluorescence screen ibid (after DMC before FM) after a slit-system.

– fluorescence screen after FM.

In addition, it is planned to have an insertable pinhole array to serve as wave front monitor to control the flatness of the wave front (and thus the energy resolution). The best place for it is with the filters. It will absorb up to 700W, but will be inserted into the beam just for seconds.

8 Preliminary considerations for endstation

- Lifting table (range 8 cm);
- Optional harmonics-rejecting mirror-system;
- A large set of reference foils;
- 3 ionization chambers; N_2, Ar, Kr gas-lines; HV supply and 3 amplifiers + VF-converters;
- Fluorescence detector (SDD) + MCA's;
- LN_2-cryostat;
- LHe-cryostat (+TEY capability);
- "goniometric head" sample holder, high accuracy vertical and lateral translation stages;

- Everything integrable into HV-system; vacuum components;
- Everything easily removable for in-situ setups;
- XMCD extension;
- XES setup; need for space(?);
- Gas connections, gas-bottles cabinets, poison-gas exhaust, sensors, etc.;
- XAFS sample preparation in close proximity to the beamline (glove box, pellet press, fume cupboards, analytical balance etc.).

References

[1] J. Juanhuix, Internal report AXD-EXBO-DG-0501, Initial XAS beamline optics design.

[2] J. Campmany, Accelerator Division, Internal report AAD-SR-ID-AN-0148.

[3] M. Sanchez del Rio, R. J. Dejus, "XOP: A Multiplatform Graphical User Interface for Synchrotron Radiation Spectral and Optics Calculations" SPIE Proc., 3152 (1997) 148; web page: http://www.esrf.fr/computing/scientific/xop2.1/.

[4] Tomoya Uruga, Hiroaki Kimura, Yoshiki Kohmura, Masanori Kuroda, Hisao Nagasawa, Kiyotaka Ohtomo, Hitoshi Yamaoka, Tetsuya Ishikawa, Tatzuo Ueki, Hitoshi Iwasaki, Shinya Hashimoto, Yasuharu Kashihara, Kazumori Okui, *X-ray optics research and development for SPring-8 beamlines*, Rev. Sci. Instrum. **66** (1995) 2254-2256.

[5] R. L. Bilsborrow, P. A. Atkinson, N. Bliss, A. J. Dent, B. R. Dobson and P. C. Stephenson, *A wide-aperture dynamically focusing sagittal monochromator for X-ray spectroscopy and diffraction*, J. Synchrotron Rad. **13** (2006) 54–58.

[6] G. M. Lamble and S. M. Heald, *Operation of a dynamically bent sagittally focusing double crystal monochromator for XAFS studies*, Rev. Sci. Instrum. **83** (1992) 880–884.

[7] MacDowell, A. A., Celestre, R. S., Howells, M. R., McKinney, W., Krupnick, J., Cambie, D., Domning, E. E, Duarte, R. M., Kelez, N., Plate, D. W., Cork, C. W., Earnest, T. N., Dickert, J., Meigs, G., Ralston, C., Holton, J. M., Alber, T., Berger, J. M., Agard, D. A. & Padmore, H. A., *Suite of three protein crystallography beamlines with single superconducting bend magnet as the source*, J. Synchrotron Rad. **11** (2004) 447–455.

[8] MPDB v6.51 – demo, JAHM Software, Inc., http://www.jahm.com.

[9] B. Lai and F. Cerrina, NIM A **246** (1986) 337–341.

[10] S. Pascarelli, T. Neisius and S. De Panfilis, Turbo-XAS: dispersive XAS using sequential acquisition, J. Synchrotron Rad. **6** (1999) 1044–1050.

[11] R. Frahm, Rev. Sci. Instrum. **60 (1989)** 2515.

[12] H. Schulte-Schrepping, W. Drube, *Properties of a detuned non-dispersive double crystal monochromator*, NIM A **467–468** (2001) 396–399.

[13] Patterson et al., NIM A **540** (2005) 42.